Proton Transport across Transient Single-File Water Pores in a Lipid Membrane Studied by Molecular Dynamics Simulations

S. J. Marrink,[*] F. Jähnig,[*] and H. J. C. Berendsen[#]

[*]Abteilung Membranbiochemie, Max-Planck-Institut für Biologie, D-72076 Tübingen, Germany, and [#]Biophysical Chemistry, University of Groningen, 9747 AG Groningen, The Netherlands

ABSTRACT   To test the hypothesis that water pores in a lipid membrane mediate the proton transport, molecular dynamic simulations of a phospholipid membrane, in which the formation of a water pore is induced, are reported. The probability density of such a pore in the membrane was obtained from the free energy of formation of the pore, which was computed from the average force needed to constrain the pore in the membrane. It was found that the free energy of a single file of water molecules spanning the bilayer is 108($\pm$10) kJ/mol. From unconstrained molecular dynamic simulations it was further deduced that the nature of the pore is very transient, with a mean lifetime of a few picoseconds. The orientations of water molecules within the pore were also studied, and the spontaneous translocation of a turning defect was observed. The combined data allowed a permeability coefficient for proton permeation across the membrane to be computed, assuming that a suitable orientation of the water molecules in the pore allows protons to permeate the membrane relatively fast by means of a wirelike conductance mechanism. The computed value fits the experimental data only if it is assumed that the entry of the proton into the pore is not rate limiting.

INTRODUCTION

The presence of ion gradients is of vital importance to the functioning of most living cells. For instance, ion gradients are required as energy sources, for signal transmission, as a way to orient proteins, and as tool to induce phase separations and fusions. Therefore, it is of key importance for the cell to be able accurately to regulate the transport of ions across the membrane. For most ions the transport across the membrane is regulated by protein systems, because the basal ion permeation process is much too slow. However, in the case of proton transport the basal permeation mechanism turns out to be much faster, and it becomes significant on the biological time scale. Electrochemical gradients of protons play a fundamental role in the case of bacteria. There have been speculations that proton gradients used by bacteria are replaced in eucaryotic cells by sodium or potassium gradients to circumvent the basal leak of protons.

Thus far, the molecular mechanism underlying the striking difference between the transport rates of protons on the one hand, and of other ions on the other hand, is not well understood. The most convincing proposal so far (Nichols and Deamer, 1980) is that a water pore might be involved, across which the protons can permeate fast by a wirelike conductance mechanism. The experimental data do not provide clear answers, however. If water pores exist, they are expected to be only transient and therefore hard to detect.

To test the hypothesis that water pores do form spontaneously in lipid membranes, and that these pores are stabi-

lized enough to account for the high proton transport rates, we extended our molecular dynamic (MD) simulations of lipid membranes (Egberts et al., 1994; Marrink et al., 1993; Marrink and Berendsen, 1994, 1996) to study the thermodynamic properties of a water pore in a membrane. We derived transport equations for the proton transport rate across water pores in the membrane, considering different possible mechanisms. The rate constants of these transport equations are amenable to computation by MD simulations.

We started from earlier simulations of a DPPC membrane including full atomic detail, which have proved to behave realistically (Egberts et al., 1994). Because the process of water pore formation is too slow to be modeled directly by MD simulations, we applied the same method as we did in the modeling of the permeation of small molecules (Marrink and Berendsen, 1994, 1996), i.e., by means of restrained dynamics. We induce the formation of a pore by slowly pulling a strand of coupled water molecules into the membrane. The stability of the pore can then be computed from the average force exerted on the constrained file of water molecules. At the same time, the dynamic and orientational behavior of the water molecules in the pore can be followed. This will allow for prediction of the rate-limiting step in the proton transport through the water pore.

The next section reviews the experimental data and the current models concerning proton transport. Thereafter, the derivation of the transport equations are given, followed by a description of the method of simulation. Finally, the results are presented and discussed.

REVIEW

Experimental measurements

Experimentally, the transport rate of ions across (model) lipid membranes can be calculated from the decay times of concentration gradients or from

conductance measurements. If the driving force is a concentration gradient Δc, the permeability coefficient P can be calculated:

$$P = J/\Delta c, \qquad (1)$$

where J is the molar ion flux per unit of surface area. Similarly, in the case of a potential difference $\Delta\phi$ as driving force, the conductance is obtained:

$$G = I/\Delta\phi = zFJ/\Delta\phi, \qquad (2)$$

where I is the current density carried by the ions of charge of z electron units. The two types of measurement are related to each other by

$$P = \frac{RT}{cz^2F^2} G, \qquad (3)$$

in which F denotes Faraday's constant.

Early experiments (Mueller and Rudin, 1967) with planar lipid membranes showed that the resistance of a lipid membrane to ionic conduction is very high. Later experiments (Hauser et al., 1973; Nozaki and Tanford, 1981) showed that the fluxes of monovalent ions are $\sim 10^{-16}$ mol cm^{-2} s^{-1}. For proton transport, values of $\sim 10^{-15}$ mol cm^{-2} s^{-1} were found (Nichols et al., 1980; Deamer and Nichols, 1983). However, the driving concentration differences in the case of ions are of the order of 0.1 M, whereas for proton transport they are only near 0.1 μM. This implies a permeability coefficient for ion transport of the order of 10^{-12} cm s^{-1}, compared with 10^{-4} cm s^{-1} for proton transport, a difference of 8 orders of magnitude. Later experiments in various laboratories confirmed the discrepancy between proton and other cation permeability coefficients, with differences of 6–8 orders of magnitude usually, depending on the details of the lipid system. Typically reported values for proton transport measurements are permeabilities of 10^{-4}-10^{-6} cm/s, corresponding to conductances of 10^{-7}-10^{-9} S/cm^2.

The anomaly of the proton transport mechanism is underlined by the observations (Deamer and Nichols, 1983; Gutknecht, 1984; Perkins and Cafiso, 1986) that the conductance is only slightly dependent on concentration (pH); the conductance increases 10-fold over a pH range of 1–11. For other ion transport processes the conductance increases linearly with concentration. Furthermore, hydroxide transport is as fast as proton transport, implying that both processes are similar.

The coupling between proton and water transport is less clear. On the one hand, experiments on membranes with varying lipid compositions indicate no coupling (Gutknecht, 1987a). On the other hand, however, temperature-dependent measurements indicate similar behavior for proton and water transport (Elamrani and Blume, 1983). Both transport processes show no maximum at the main phase transition, in contrast to the temperature dependence of ion transport.

The experimental evidence thus clearly suggests an anomalous permeation process for protons across lipid membranes. Below, three different models are discussed that attempt to account for the observed experimental data.

Solubility–diffusion model

In the simplest version of the model, the homogeneous solubility–diffusion model, it is assumed that the transport rate of a permeant is proportional to the product of the solubility coefficient and the diffusion constant of the permeant in the membrane.

In the case of ions, the solubility coefficient can be estimated from the Born (free) energy of the ion in the membrane. Assuming a dielectric constant $\epsilon_r = 2$ in the membrane, Parsegian (1969) showed that the Born energy for a monovalent ion is in the range of 160 kJ/mol, an energy level never attained under physiological conditions. The Born energy of hydrated ions is more realistic, ~ 80 kJ/mol. Size-dependent measurements suggest that the permeating entity is indeed a hydrated ion (Georgallas et al., 1987). Assuming a "typical" diffusion constant of the order of 10^{-5} cm s^{-1}, the predicted transport rates are then still too low by some 3 orders of magnitude in the case of sodium (Hauser et al., 1973). Transport of

protons, which require similar Born energies to enter the bilayer as hydronium ions, cannot be understood at all with this model.

Deamer and Bramhall (1986) assumed that transient defects are present, which facilitate the solubility step. Strands of water penetrating the bilayer could reduce the energy barrier significantly. This would also explain the large increase in ion permeability at the main phase transition, when defects are more likely to be present. Modeling the membrane in more detail, Flewelling and Hubbell (1986) showed that the dipole energy lowers the Born energy significantly, thus facilitating the permeation of ions. Moreover, they showed that this effect is largest for anions, which are known to permeate the bilayer faster than cations do.

Although the transport rates of ions can be better understood if one takes into account the molecular details, i.e., with an inhomogeneous solubility–diffusion model, in the case of protons the solubility–diffusion model is not sufficient. Predicting proton transport rates seems to require more-elaborate defects.

Weak-acid model

In the weak-acid model, proposed by Gutknecht and Walter (1981), it is assumed that the high proton transport rate is due to weakly acidic contaminants, which act as proton carriers (protonophores). Therefore, the anomalously high permeation rate of protons across lipid bilayer membranes would be mainly an experimental artifact and not an intrinsic property of the bilayer itself. The presence of trace contaminants is very likely, considering the conditions under which lipid bilayers are prepared for study. Lipid hydrolysis and lipid oxidation are considered to be possible origins for weak-acid protonophores.

Experimental evidence supporting this model comes from the observations (Cafiso and Hubbell, 1983) that the rate of proton transport decreases if extra care is taken to reduce possible sources of contaminants. On the other hand, the rate of proton transport increases in systems that are more labile to hydrolysis or oxidative damage. Further evidence has been obtained by showing that proton permeability decreases on addition of bovine serum albumin, a strong contaminant binding agent (Gutknecht, 1987a). Addition of fatty acids, which can act as protonophores, showed the opposite effect.

Although the experimental data clearly show that protonophores indeed are a possible transport mechanism for protons, the difference of 6–8 orders of magnitude between proton and other cation permeabilities cannot be accounted for; at most, 1–2 orders of magnitude can be accounted for. Furthermore, the pH dependence of protonophores is considerably different from the pH dependence of proton conductance. Therefore an additional mechanism for proton transport is required.

tHBC model

The transient hydrogen-bonded chain (tHBC) model was proposed by Nagle (1987) and is based on the earlier proposal of hydrogen-bonded chains associated with proteins (Nagle and Morowitz, 1978) and the assumption that, because of thermal fluctuations, a strand of water molecules can connect through the membrane to the opposing water layer, thus forming a water pore (Nichols and Deamer, 1980). According to the tHBC model, when a pore has formed, protons can be transported very fast by a combined mechanism, similar to that of proton mobility in ice (see Fig. 1).

In this mechanism, first an ionic defect is transported, by means of a hopping mechanism, followed by the transport of a turning defect. Both steps could in principle transport part of the total charge. After the second step, another proton could be transported by the same mechanism. The same mechanism accounts for the high proton mobility in water as well, which is ~ 7 times faster than the mobility of other ions. In ice, proton mobility is even faster, with the ionic defect hopping at a rate of $\sim 10^{11}$ s^{-1}. The turning defect, requiring larger reorganizations, is at least 2 orders of magnitude slower (Pines and Huppert, 1985).

Recent computer simulations (Pomès and Roux, 1996a,b), which used a combined quantum-classical approach to study the dynamics of proton
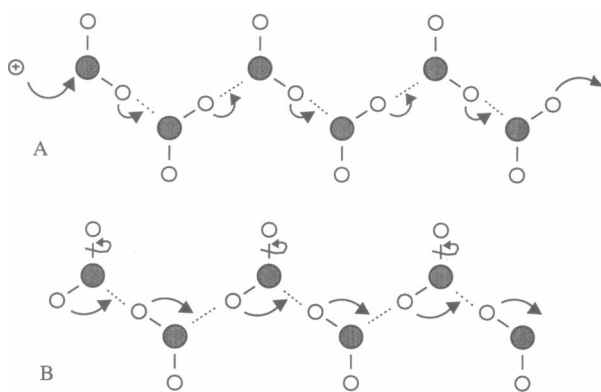
FIGURE 1   Transport of (A) the ionic defect and (B) the turning defect along a hydrogen-bounded chain of water molecules.

translocation across a water wire, showed that the actual process is neither a hopping nor a totally concerted mechanism but involves cooperative behavior of as many as five neighboring water molecules. Protons can be translocated over these distances within less than 1 ps. This study clearly indicates that the translocation step of protons along a water wire can be very fast, probably even faster than in ice. A subsequent study of a water wire inside a gramicidin channel further showed that the rate of the turning defect depends very much on the local environment of the water molecules. If the interactions between the water wire and the surrounding (i.e., channel) atoms are weak, the rate of turning defect translocation can also be very fast (picosecond time scale); however if (part of) the water molecules are strongly coupled (by hydrogen bonding or electrostatic interactions), the rate may slow down beyond the nanosecond time scale.

Evidence for the tHBC mechanism in membranes comes from the comparison of proton transport rates through gramicidin channels, which are known to have a single wire of water molecules. Various experiments (e.g., see the review of Deamer, 1987) indicate that gramicidin channels also show an anomalous proton transport. Moreover, the proton transport is uncoupled to the transport of water or to other ions, which suggests that the protons are able to move fast along associated hydrogen bonds. However, the observation that a partial substitution of D_2O for H_2O does not result in a significant decrease of proton transport in membranes, but does so in the presence of gramicidin channels, indicates that the water wire in both systems cannot be completely the same (Deamer, 1987). Also, the clear pH dependence observed for proton transport through gramicidin channels (Gutknecht, 1987b) indicates a different mechanism. One possibility would be that more than one strand of water molecules forms a water pore, offering alternative routes for the proton transport. A pore with fluid water can be ruled out, as it would offer fast permeation routes to other ions as well.

Other interesting data form the experimental measurements of the permeation rates of various ions across model membranes (Hamilton and Kaler, 1990) and of the permeation rates of ions and protons across lipid bilayers with increasing thickness (Deamer et al., 1995; Paula et al., 1996). Fitting the experimental data to a simplified pore model yields evidence for the existence of water pores conducting ions, at least in thin membranes, and of protons in membranes with chain lengths up to 22.

Depending on which step is considered to be rate limiting in the total transport process, the tHBC model can be further subdivided into three different models (Nagle, 1987). Each of these models easily yields a constant conductance as a function of pH, which one requires to fit the experimental data. The first model assumes that the pore exists long enough to conduct several protons. The pH independence follows then from the assumption that the transport of the turning defect is rate limiting. This is in agreement with the results of studies in ice, which indicate that the turning defect is an order of magnitude slower than the hopping defect (Nagle and Tristam-Nagle, 1983). The second model assumes that the pore is relatively short lived and conducts at most one proton. The transport of a turning defect, in which a hydrogen bond is broken (see Fig. 1), is

considered to be destructive for the whole pore. If the rate-limiting step of the proton permeation process is now the formation of the (very transient) pore, then this model also predicts a constant conductance versus pH. In the third version of the model it is assumed that proton transport takes place when two opposing strands meet each other; one of the strands carries a proton, the other a hydroxyl ion, which on recombination results in a net transport of protons. A pH independence is obtained if the probability of recombination is much larger than the probability of transfer of a proton between a neutral chain and one that has an excess (or deficit) proton.

Whether the proton transport rate that is predicted by these tHBC models is large enough to account for the experimental data depends primarily on the probability that pores are formed. Assuming that the rate-limiting step is formed by the transport of the turning defect (model I), Nagle (Deamer and Nichols, 1989) calculated a pore density of 2×10^4 cm^{-2} bilayer area required for fitting the lower limit conductance data of Gutknecht (1987a). Comparing this value with the solubility of single water molecules in bulk alkane phases means that, on average, only 1 water molecule of 10^6 dissolved water molecules is required to take part in the pore. This result is similar to the result estimated from proton conductance through gramicidin channels (Gutknecht, 1987a). It implies that such a rare process as the formation of a complete pore can in principle be sufficient to account for the high proton transport rate. The fact that water pores are never observed experimentally is in agreement with the low probability of pore formation.

The three different types of tHBC model can be distinguished by investigating the exact curve shapes of plots of proton conductance versus potential difference or pH gradients across the membrane. Nagle (1987) derived equations for all three tHBC models, relating proton flux to driving force. The predicted curve shapes range from sublinear to superlinear. These predictions were tested by Deamer and Nichols (1989), who used many different experimental data. They concluded that the third model is most probable; the second model, the least. However, some of the experimental data appeared to be conflicting, and no conclusive evidence was obtained. Besides, the theoretically predicted curve shapes depend quite critically on the precise shape of the free energy profile of proton solvation into the pore.
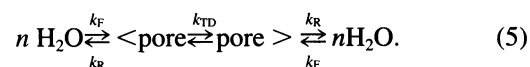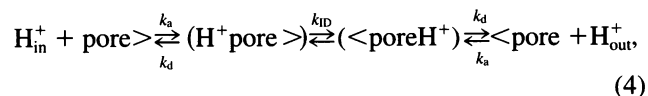
THEORY

We now derive a general version of the tHBC model. The equation for the transport rate of protons that is derived can be tested by computation with the molecular dynamics technique.

General tHBC model

We restrict the description to the transport of protons only and neglect the contribution of hydroxide ions; i.e., we consider low pH. However, similar equations can be derived for the transport of hydroxide ions, which will dominate the transport at high pH. Furthermore, we are interested only in the linear regime of small concentration differences Δc, where Fick's law $J \sim \Delta c$ holds and second-order terms can be neglected.

The set of kinetic equations describing the proton transport across a water pore is as follows:

$$H_{in}^+ + pore > \underset{k_d}{\overset{k_a}{\rightleftarrows}} (H^+ pore >) \overset{k_{ID}}{\rightleftarrows} (<poreH^+) \underset{k_a}{\overset{k_d}{\rightleftarrows}} <pore + H_{out}^+, \tag{4}$$

$$n\ H_2O \underset{k_R}{\overset{k_F}{\rightleftarrows}} <pore \overset{k_{TD}}{\rightleftarrows} pore > \underset{k_F}{\overset{k_R}{\rightleftarrows}} n H_2O. \tag{5}$$

In Eqs. 4 and 5, pore> represents a water pore in the membrane that has the required conformation to transport a proton from the inside to the outside the cell and <pore represents the conformation suitable for transporting protons in the opposite direction. (H^+pore>) and (<poreH^+) denote the intermediate complexes in which the proton is associated with either side of the pore opening. Rate constants k_{TD} and k_{ID} describe the kinetics of transport of the turning and the ionic defect, respectively. The kinetics of the reversible formation of a water pore out of n water molecules is described with rate constants k_F (formation) and k_R (reduction) and the proton–pore association equilibrium with rate constants k_a (association) and k_d (dissociation). Both pore conformations are considered to have the same rate constants.

The kinetics of transport of the ionic defect requires the entering of a proton at the pore opening, and therefore the total rate law (Eq. 4) is second order, i.e., it depends on the proton concentration. To simplify the equations, we will use a second-order rate constant k_2 to describe the total rate law:

$$\text{pore>} + H_{in}^+ \overset{k_2}{\rightleftharpoons} \text{<pore} + H_{out}^+, \qquad (6)$$
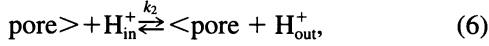
with $k_2 = k_{ID} k_a/(k_d + k_{ID})$. Two limits can be distinguished. If the ionic translocation step is much faster than the dissociation step, i.e. $k_{ID} \gg k_d$, then $k_2 = k_a$. In this case the total rate law is diffusion controlled. In the other case, if $k_{ID} \ll k_d$, then $k_2 = k_{ID} k_a/k_d$, and the rate law is activation controlled.

From the above kinetic equations, the following flux equations can be derived:

$$\frac{d[H^+]}{dt} = k_2([\text{pore>}][H^+ + \Delta H^+] - [\text{<pore}][H^+]), \qquad (7)$$

$$\frac{d[\text{pore>}]}{dt} = -k_2([\text{pore>}][H^+ + \Delta H^+] - [\text{<pore}]$$

$$(8)$$

$$\cdot [H^+]) - k_{TD}([\text{pore>}] - [\text{<pore}]) - k_R[\text{pore>}] + k_F,$$

$$\frac{d[\text{<pore}]}{dt} = -k_2([\text{<pore}][H^+] - [\text{pore>}][H^+ + \Delta H^+])$$

$$(9)$$

$$- k_{TD}([\text{<pore}] - [\text{pore>}]) - k_R[\text{<pore}] + k_F,$$

where we have considered a proton concentration $[H^+{}_{in}] = [H^+ + \Delta H^+]$ at the inside and a proton concentration $[H^+{}_{out}] = [H^+]$ at the outside. (Note that we have incorporated the bulk water concentration into k_F.)

In the steady state, the concentration of pores oriented in both directions will be constant, implying that both Eqs. 8 and 9 become zero. From this the following relationship results:

$$[\text{<pore}] = 2k_F/k_R - [\text{pore>}]. \qquad (10)$$

Now the pore concentrations can be expressed in terms of rate constants and proton concentrations only and can be substituted into Eq. 7. The resulting expression for the proton transport rate is then given by

$$J_{protons} = \frac{d[H^+]}{dt} = \frac{k_2 k_F(2k_{TD} + k_R)}{k_R(2k_2[H^+] + 2k_{TD} + k_R)}[\Delta H^+]$$

$$(11)$$

$$+ O\{[\Delta H^+]^2\}.$$

This equation describes the proton flux that results from a pH gradient. When the pH difference is small, the second-order terms can be neglected, and the flux is linear with the applied concentration difference. Recalling Eq. 3, one sees that the flux resulting from a potential difference is related to the flux resulting from a concentration difference through an additional multiplication by the proton concentration. For the proton conductance to become independent of proton concentration it is required that Eq. 11 become inversely proportional to the proton concentration. This is achieved only if the first term of the denominator, $k_2[H^+]$, is much larger than the other two terms, i.e., if the transport of the proton across the pore is not the rate-limiting step. Then Eq. 11 simplifies to

$$J_{protons} = \frac{k_F(2k_{TD} + k_R)}{2k_R[H^+]}[\Delta H^+] + O\{[\Delta H^+]^2\}. \qquad (12)$$

Now, if the stability of the pore is much larger than the transition time of the turning defect, i.e., $k_{TD} \gg k_R$, then Eq. 12 corresponds to tHBC model I. In the case that $k_R \geq k_{TD}$, the pore is short lived and conducts at most one proton, corresponding to tHBC model II.

The third tHBC model follows from a different kinetic mechanism, in which proton transport results from the recombination of a proton–hydroxide pair. In this case kinetic equation 6 is replaced by a third-order rate law (depending on both proton and hydroxide concentration):

$$\text{pore>} + H_{in}^+ + OH_{out}^- \overset{k_3}{\rightleftharpoons} \text{<pore} + H_2O, \qquad (13)$$
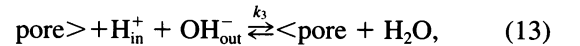
with third-order rate constant k_3. This kinetic equation actually describes the water dissociation equilibrium across the pore. It also combines the association and ionic translocation steps. Note, however, that the rate constant for the translocation of the ionic defect, k_{ID}, is not necessarily the same for the recombination mechanism as for the single uncoupled mechanism.

The flux equations now become

$$\frac{d[H^+]}{dt} = k_3([\text{pore>}][H^+ + \Delta H^+]\frac{K_w}{[H^+]}$$

$$(14)$$

$$- [\text{<pore}] [H^+]\frac{K_w}{[H^+ + \Delta H^+]}),$$

$$\frac{d[\text{pore}>]}{dt} = -k_3\left([\text{pore}>][H^+ + \Delta H^+]\frac{K_w}{[H^+]}\right.$$

$$\left. - [<\text{pore}][H^+]\frac{K_w}{[H^+ + \Delta H^+]}\right. \tag{15}$$

$$\left. - k_{TD}([\text{pore}>] - [<\text{pore}]) - k_R[\text{pore}>] + k_F,\right.$$

$$\frac{d[<\text{pore}]}{dt} = -k_3([<\text{pore}][H^+]\frac{K_w}{[H^+ + \Delta H^+]}$$

$$- [\text{pore}>][H^+ + \Delta H^+]\frac{K_w}{[H^+]}) - k_{TD}([<\text{pore}] \tag{16}$$

$$- [\text{pore}>]) - k_R[<\text{pore}] + k_F,$$

where K_w stands for the water dissociation constant. When steady-state conditions are applied, the flux can be expressed (similarly to Eq. 11) as

$$J_{\text{protons}} = \frac{k_3 K_w k_F(2k_{TD} + k_R)}{k_R[H^+](2k_3 K_w + 2k_{TD} + k_R)}[\Delta H^+] + O\{[\Delta H^+]^2\}. \tag{17}$$

With the recombination mechanism the conductance is always independent of the proton concentration, no matter what the rate-limiting step is. tHBC model III can be recovered with the following two assumptions. First, the pore is considered to be very transient and allows for only one recombination step. This means that $k_R \geq k_3 K_w$, and Eq. 17 reduces to

$$J_{\text{protons}} = \frac{k_F k_3 K_w}{2k_R[H^+]}[\Delta H^+] + O\{[\Delta H^+]^2\}. \tag{18}$$

The second assumption is that the recombination mechanism dominates the first mechanism; otherwise the conductance becomes dependent on proton concentration again. This assumption is achieved when $k_3 K_w > [H^+]k_2$. This implies that, at normal pH values, the translocation step coupled to the recombination of a proton–hydroxide pair is required to be orders of magnitude faster than the uncoupled translocation step.

In the original description of Nagle's model III it is presumed that the pore forms through the connection of two strands, each penetrating the membrane halfway. In the above derivation of the same model this is not a necessary condition, and therefore the model is more general. In fact, two other models can be deduced from Eq. 17. If $k_3 K_w$ is much larger than the other two terms in the denominator, Eq. 17 becomes equal to Eq. 12, from which models I and II could be derived. If $k_3 K_w > [H^+]k_2$ the proton transport is dominated by the recombination mechanism, resulting in models Ia and IIa.

METHOD OF SIMULATION

To test which of the mechanisms described in the previous section, if any, could serve as a realistic model for proton

transport across a membrane, one needs an estimate for k_F, the rate of pore formation; k_R, the rate of pore reduction, k_{TD}; the rate of transport of the turning defect, k_{ID}; the rate of transport of the ionic defect; and $k_{a/d}$, the proton–pore association–dissociation rates.

This section describes how the transport process of protons through water pores spanning a lipid membrane can be computed from MD simulations. The method of the simulation of the membrane, the method of simulating the water pore, and the methods of calculation of the various rate constants from the simulation data are described in turn.

Membrane

The simulated system is equal to the system used in the previous studies (Egberts et al., 1994; Marrink and Berendsen, 1994, 1996), i.e., a periodic box containing 64 DPPC and 736 water molecules (SPC), arranged in a bilayer conformation. The system was coupled to a constant temperature (350 K) and a constant pressure (1 atm). The membrane phase is the biologically relevant liquid-crystalline phase. The simulation parameters and the force field are identical to those used in the simulation of water permeation (Marrink and Berendsen, 1994). In this study the interaction parameters between water and lipid membrane interior (which are important for the present study as well) were chosen from optimized decane–water interaction parameters. We obtained an equilibrated membrane system by using the last time frame of these simulations.

To study the formation of a hydrogen-bonded chain of water molecules in the membrane we performed two separate MD simulations of more than 1 ns each, with constrained dynamics of the water molecules in the pore. Also, several short runs were performed in which the constraints were removed (see Results). The simulations were carried out on a Cray-YMP supercomputer, with a speed of 5 ps/h of CPU time.

Water pore

In our simulation studies of the permeation of water molecules (Marrink and Berendsen, 1994) we constrained single water molecules inside the membrane because the spontaneous entering of a water molecule in the membrane is too slow to be studied on a MD time scale. The formation of a membrane-spanning water pore, consisting of ~20 water molecules, will be even much slower. Therefore, a water pore has to be induced into the membrane by means of a set of suitable constraints. The most straightforward method would be to constrain a set of water molecules in the conformation of a pore. This could be done by resetting the z coordinates of the centers of mass of the water molecules in each step to their original, constrained values z_j. In applying this method, the problem arises of choosing the constrained positions of the water molecules, e.g., their mutual distances. Besides, additional constraints in the xy

plane would be necessary to restrain the individual water molecules from breaking away. To restrict the essential phase space of the strand as little as possible, one would rather like to have a set of dynamic constraints, which would allow the strand to take nonlinear conformations and also allow individual water molecules to rotate. This can be achieved by modifying the Hamiltonian of the system by adding an additional potential, which couples a strand of $N' - 1$ water molecules to another water molecule that is constrained at position z (see Fig. 2). Now we can induce a water pore in the membrane by slowly changing the constraint position of the water molecule to which the other water molecules are coupled.

The coupling potential $V_{couple}(r_{ij})$ acting between the $N' - 1$ neighboring water pairs ij in the pore was chosen to be harmonic for distances r_{ij} larger than some cutoff distance r_{couple}. To prevent the coupling forces from becoming too large, a second cutoff radius is introduced beyond which the potential increases linearly instead of quadratically:

$$V_{couple}(r_{ij}) \quad = 0 \quad\quad 0 < r_{ij} < r_{couple}$$

$$= \frac{1}{2} K_{couple}(r_{ij} - r_{couple})^2 \quad r_{couple} < r_{ij} < r_{couple} + \Delta r_{harm}$$

$$= K_{couple}\left(r_{ij} - r_{couple} - \frac{1}{2}\Delta r_{harm}\right)(\Delta r_{harm}) \quad r_{couple} + \Delta r_{harm} < r_{ij}.$$

(19)

The values for the parameters are to some extent arbitrary and had to be optimized during some test runs. The criterion that we used for the optimization was to ensure that the water pore was hydrogen bonded most of the time, the restraints being as small as possible. The distance at which the restraining potential is felt was finally set to $r_{couple} = 0.34$ nm, which corresponds to the first maximum in the radial distribution function of SPC water. Water molecules that are separated by larger distances interact only weakly and tend to destabilize the pore. Test runs with larger coupling distances resulted in water pores that were much less hydrogen bonded. The restraining potential is chosen to

be harmonic over a distance of $\Delta r_{harm} = 0.2$ nm. The choice of Δr_{harm} turned out not to be very critical; because of the weak force constant, $K_{couple} = 60$ kJ mol^{-1} nm^{-1}, the coupling forces remain small. Larger values for the force constant restrained the pore too much; smaller values did not match the hydrogen-bonding criterion.

One additional problem arose when in some test runs the complete set of coupled water molecules detached itself from the water layer and dissolved into the membrane. Therefore, the z position of the last coupled water molecule (which initially resides in the water layer) was coupled to its original position z_0 to prevent the pore from dissolving completely. The coupling potential was taken infinitely narrow, i.e., as a constraint.

The number of coupled pore molecules between the water molecule constrained in the membrane and the one constrained in the middle of the water layer was chosen such as to allow for a fully hydrogen-bonded chain that could still adopt some nonlinear conformations. In practice approximately four additional (i.e., not necessary in a fully stretched conformation) water molecules were coupled. The length of the pore thus increased from initially eight water molecules residing in the water layer to finally nineteen water molecules in the full pore conformation, i.e., two constrained ones and seventeen coupled between them.

Rate of pore formation

Consider the probability $p(z)$ that a single file (or strand) of water molecules penetrates the membrane up to position z along the membrane. Assuming Boltzmann statistics, this probability will be related to its free energy of formation ΔG_{strand} by

$$p_{strand}(z) \sim \exp(-\Delta G_{strand}(z)/kT). \quad (20)$$

In the limit of z reaching z_2, the position in the bulk water phase at the opposite site of the membrane, the free energy difference applies to a complete water pore spanning the bilayer (ΔG_{pore}), and from Eq. 20 p_{pore} can be computed. The rate of pore formation then follows from

$$k_F \sim k_R p_{pore} \sim k_R \exp(-\Delta G_{pore}/kT), \quad (21)$$

where k_R is the rate of pore reduction (see the next subsection).

It is possible to determine directly the derivative of $\Delta G_{strand}(z)$ by measuring the average force exerted on a strand of water molecules that is constrained at a depth z in the membrane. This is shown in the following derivation. Consider a system with N particles, of which one is constrained at a position z'; then

$$\frac{d\Delta G(z)}{dz} = -\frac{RT}{Q'(z)}\frac{dQ'(z)}{dz}, \quad (22)$$
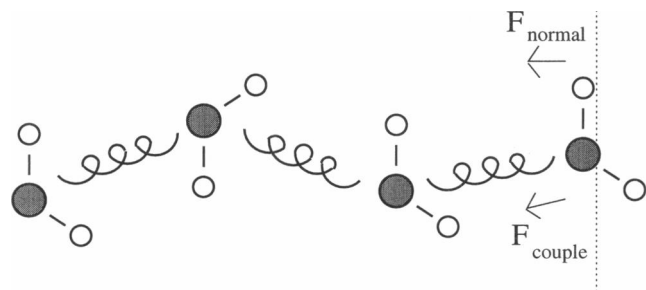

FIGURE 2 Coupled strand of water molecules. The dashed plane indicates the plane at position z in the membrane to which the leading water molecule is constrained. The springlike curves denote the harmonic coupling potentials between the pore molecules. The forces F_{couple} and F_{normal}, acting on the constrained water molecule, are required for the computation of the free energy of pore formation (see the next subsection).

where Q' is the constrained partition function of the system:

$$Q'(z) = a \int dr_1 \ldots r_N \, \delta(z - z') \exp(-V(r_1 \ldots r_N)/kT).$$

(23)

The derivative of Q' is found by partial integration of Eq. 23 to be

$$\frac{dQ'(z)}{dz} = -\frac{a}{kT} \int dr_1 \ldots dr_N \, \delta(z - z') \frac{\partial V}{\partial z} \exp(-V/kT).$$

(24)

Hence

$$\frac{d\Delta G(z)}{dz} = N_{Av} \left\langle \frac{\delta V(r_1 \ldots r_N)}{\delta z} \right\rangle = N_{Av} \langle F_z(z) \rangle,$$

(25)

where $\langle F_z(z) \rangle$ is the mean force on the constraint (i.e., the component of the force on the constraint water molecule in the direction of the constraint z, averaged over the constraint ensemble). On integration of Eq. 25, the required potential of mean force for a strand of water molecules, $\Delta G_{strand}(z)$ in Eq. 20, can be constructed.
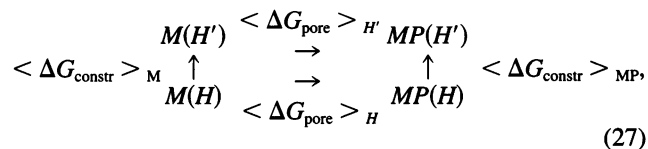
The mean force on the constraint can be monitored during the constrained simulation of the water pore as described above. The required force consists of two terms, a coupling force that arises from the connection with the other pore molecules and a normal force that is due to the standard force field (see also Fig. 2):

$$\langle F_z(z) \rangle = \langle F_z^{normal,N'}(z) + F_z^{coupled,N'-1 \to N'}(z) \rangle.$$

(26)

The first part of the free energy curve, where z remains within the area of nonzero water density (i.e. regions 1 and 2 as defined in the four-region model (Marrink and Berendsen, 1994; Marrink, 1994) of the lipid membrane), can be obtained directly from the free energy of a single water molecule, which we have already computed accurately (Marrink and Berendsen, 1994). We have shown that in regions 1 and 2 the water molecules remain hydrogen bonded with at least one other water molecule. Therefore the excess free energy of a single water molecule equals that of a strand of connected water molecules in the hydrophilic regions of the membrane. We will use the coupling method only for strands that penetrate further into the membrane and combine these data with the previously computed data to construct the complete free energy profile.

Note that the ensemble for which the potential of mean force is valid is the ensemble to which the modified Hamiltonian applies (i.e., the Hamiltonian including the coupling potential). Inasmuch as one is actually interested in the properties of the water pore in the ensemble with an unmodified Hamiltonian, it is necessary to estimate the free energy cost involved in the modification. One could calculate this correction term by using the following thermody-

namic cycle:

$$\langle \Delta G_{constr} \rangle_M \begin{array}{c} M(H') \xrightarrow{\langle \Delta G_{pore} \rangle_{H'}} MP(H') \\ \uparrow \qquad\qquad \uparrow \\ M(H) \xrightarrow[\langle \Delta G_{pore} \rangle_H]{} MP(H) \end{array} \langle \Delta G_{constr} \rangle_{MP},$$

(27)

in which M denotes the membrane ensemble without a pore, MP the ensemble in which a full pore is present, and H and H' the unmodified and modified Hamiltonians, respectively. The required free energy correction $\Delta(\Delta G_{corr})$, the difference between the free energy differences of creating the pore in the modified and the unmodified ensembles, is then given by

$$\Delta(\Delta G)_{corr} = \langle \Delta G_{pore} \rangle_{H'} - \langle \Delta G_{pore} \rangle_H$$

$$= \langle \Delta G_{constr} \rangle_{MP} - \langle \Delta G_{constr} \rangle_M.$$

(28)

The free energy differences ΔG_{constr} in ensembles M and MP denote the free energy cost of adding the constraints to the pore molecules in the initial and the final conformations of the water pore, respectively. The initial conformation of the pore means that all pore molecules are still dissolved in the water layer. Both free energy costs can in principle be calculated by use of a perturbation scheme in which the springs are slowly turned on and off. These are time consuming, however, and for the current study likely to be irrelevant: we expect that both terms in Eq. 28 will largely cancel. The average enthalpy of the springs will be close to 0.5 kT in both conformations; also, the entropy difference is not likely to be large, as the pores in both conformations are rather short lived. The remaining correction term will certainly be small compared with the total free energy cost of pore formation and will presumably remain within the computed uncertainty of ± 10 kJ/mol. However, we will verify these assumptions in a future study by calculation of the exact correction term.

Rate of pore reduction

The rate of pore reduction can be obtained by computing the time over which the pore is stable. This lifetime of the water pore can be estimated from a simulation in which all constraints of the full water pore are relaxed. Performing this computation for a few different pore conformations, one gets an idea about the average time over which the pore remains stable, which is inversely proportional to the reduction rate k_R.

Rate of ionic translocation

Because the translocation process of a proton across a water pore involves the formation and breaking of OH bonds, it cannot be modeled in a classical way by means of MD simulations. However, an estimate of the rate of ionic translocation can be derived, considering that the ionic translo-

cation step can be described as a hopping of a proton across a series of activation energy barriers that result from the breaking and forming of hydrogen bonds along the hydrogen-bonded chain. The kinetic aspects of this step have been studied extensively (Nagle et al., 1980), based on the hopping rates in ice, which are derived from phenomenological theory and experiment. The translocation rate is shown to depend on the details of the total free energy barrier of proton solvation in the pore. For a free energy barrier that is large compared with the activation energies of the hopping process, the translocation across the increasing part of the free energy barrier will be rate limiting, and the overall rate constant k_{ID} for the ionic translocation is given by

$$k_{ID} = k_{ice} < \exp(-\Delta G_{prot}(z)/kT) >, \qquad (29)$$

in which k_{ice} is the rate constant for the ionic translocation step of protons in ice ($\approx 10^{11}$/s) and $\Delta G_{prot}(z)$ is the excess free energy of solvation of a proton in the pore. The angle brackets denote an average value across the membrane.

In the case of tHBC models Ia, IIa, and III, the ionic translocation step results from the recombination of a proton and a hydroxide ion that enter the pore from opposite sides. Nagle (Nichols and Deamer, 1980) assumes that the rate constant governing this step can be much faster because of the annihilation of charge. Especially in the membrane interior, where the charge density is low, this could be a major speed-up factor.

The solvation energy $\Delta G_{prot}(z)$ has to be evaluated as a function of position z across the membrane, because the water pore will most probably not be homogeneous at all. Of course one could use MD simulations to construct the potential of mean force for the solvation of a proton (or a hydronium ion) in the pore that are similar to the methods used for the single water molecules in the membrane and the pore itself. However, this will cost a great deal of additional simulation time and will probably not be very important for the total transport rate. As a useful estimate we will use the Born energy for a proton inside a water pore in the membrane. Assuming a dielectric constant for the water pore of $\epsilon_r = 80$, surrounded by a dielectric medium with $\epsilon_r = 2$ modeling the hydrocarbon interior, Parsegian (1969) showed that the excess Born energy $\Delta H_{Born}(z)$ is given by the relation

$$\Delta G_{prot}(z) \approx \Delta H_{Born}(z) = \frac{Cq^2}{d_{pore}(z)}, \qquad (30)$$

in which d_{pore} is the diameter of the water pore, which in principle depends on the membrane position z. The width of the water pore along the membrane can be obtained directly from the simulations. C is a constant that depends on the relative dielectric constants of the water pore and the surrounding membrane. With the dielectric constants mentioned above, $C = 0.16$ (Parsegian, 1969). The electric charge of the proton, q, is not necessarily equal to e. Studies of proton translocation in ice (Scheiner and Nagle, 1983) reveal that only a fraction of $0.62e$ is carried by the ionic

translocation step; the remainder, by the translocation of the turning defect.

Rate of proton–pore association–dissociation

Assuming a random diffusive motion for the proton, and a steady pore with openings ($z = 0$) diameter $d_{pore}(0)$, the rate of proton–pore association k_a is approximately given by

$$k_a = 2\pi d_{pore}(0)D_{prot}N_A, \qquad (31)$$

where N_A is Avogadro's constant and D_{prot} denotes the diffusion constant of protons in water, which is of the order of 10^{-4} cm^2 s^{-1}. The width of the pore opening can be estimated from the simulation results.

The rate of proton–pore dissociation can also be expressed in terms of the proton diffusion rate and the pore opening diameter:

$$k_d = 24D_{prot}/\pi[d_{pore}(0)]^2. \qquad (32)$$

Note that this expression is valid only with the assumption that the pore–proton complex is not additionally stabilized.

Rate of turning defect translocation

Considering the reorientation times of water molecules (of the order of a few picoseconds), it is reasonable to assume that we will observe a large ensemble of pore conformations during the (constraint) simulations. From this we can directly estimate the transition time between the conformations. The transition time between a pore that is fully oriented in one direction and a pore that is fully oriented in the other direction determines the overall rate constant for the turning defect translocation, k_{TD}.

RESULTS

Formation of the water pore

The water pore was induced in the membrane as described in the previous section. We selected the positions of the initial strand of water molecules by choosing the largest spontaneous fluctuation that was present in the starting configuration of the membrane system. For the second simulation the largest fluctuation at the opposite side of the membrane was chosen as a starting point. Most of the results of both independent simulations turned out to be comparable.

The pulling of the strand into the membrane was performed stepwise, in nine different stages. Each stage consisted of an elongation step, a perturbation step, and a sampling period. In the elongation step the length of the coupled strand of water molecules was adjusted so the next conformation could be adopted (i.e., one or sometimes two water molecules were added in the middle of the water layer to the strand). The next conformation was attained through the perturbation step, lasting 20 ps, in which the constrained
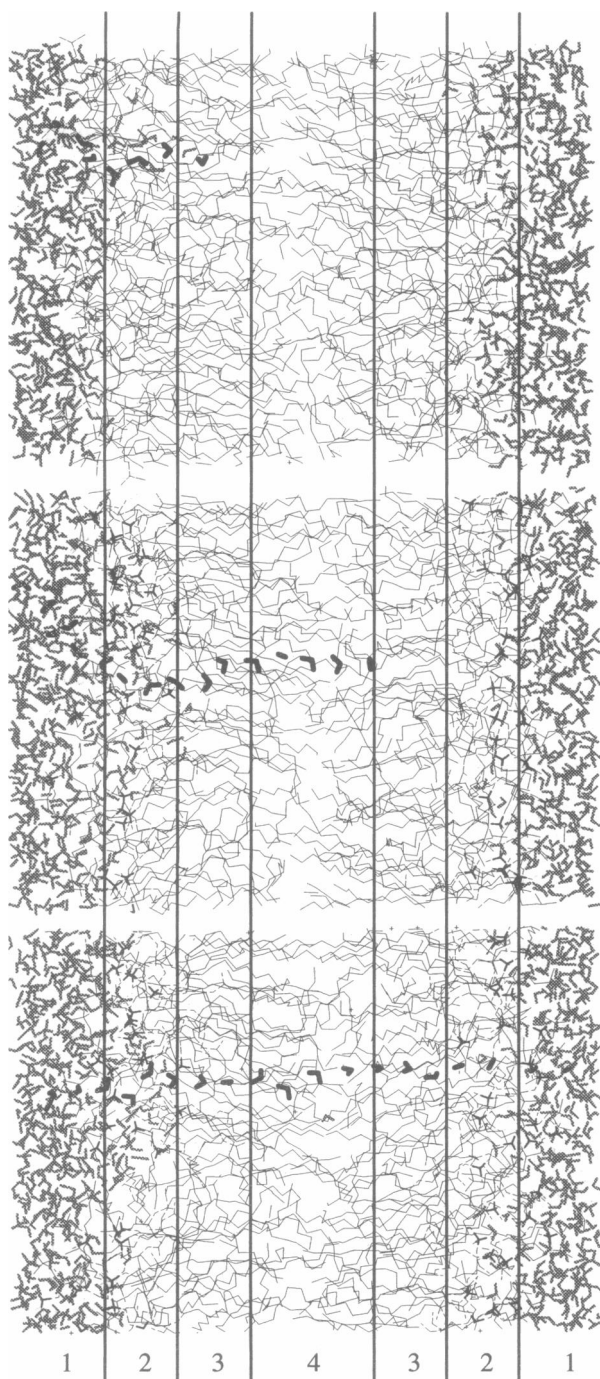
FIGURE 3 Snapshot of the water pore during the process of formation. The pore molecules are drawn with bold black lines; the other water molecules, in lighter lines. The four different membrane regions (small headgroup density, large headgroup density, large tail density, and small tail density, shown in sections 1, 2, 3, and 4, respectively), as defined elsewhere (Marrink and Berendsen, 1994; Marrink, 1994), are also indicated. The upper figure shows the pore after stage 1, the middle figure after stage 5, and the lower figure after the final stage, 9.

position $z_j(t)$ of the leading water molecule was changed linearly from the initial position $z_j(t_0)$ to a position $z_j(t_0) + \Delta z$ in the membrane. This perturbation step was followed by a sampling period of 100 ps in which the forces and coor-

dinates of the pore molecules were collected. The total simulation time to create a full pore was $9 \times 120 = 1080$ ps. For simulation 1, the initial position $z_j(t_0)$ was 1.1 nm. With Δz set to 0.45 nm, the coordinate that was finally reached was $z_j(t_{1080}) = 5.42$ nm, well into the opposite water layer (note that during the run the box length increased from 5.4 to 5.6, implying a scaling of all positions including the constrained positions of the outer two pore molecules). The corresponding parameters of simulation 2 were $z_j(t_0) = 4.25$ nm, $\Delta z = -0.45$ nm, and $z_j(t_{1080}) = 0.31$ nm.

Three stages of the pore formation process in simulation 1 are plotted in Fig. 3. The figure shows that the full water pore that is finally created indeed has a minimum conformation (i.e., fully hydrogen bonded), which could in principle allow for a fast transport of protons through the hydrogen-bonded chain. The observed (partial) pore conformations were mostly linear, with only small bends. The appearance of big loops or twisted conformations was rare. From a free energy point of view this is clear, for a linear conformation requires the least number of water molecules entering the hydrophobic core. Besides, the lipid tails are oriented perpendicular to the membrane surface. The lipid tails adjacent to the water pore showed a small preference toward even more stretched conformations, thus enhancing favorable short-range interactions between the water pore and the membrane. As a direct consequence, the box dimension in the perpendicular z direction increased during the formation of the full pore from 5.4 to 5.6 nm (simulation 1) and to 5.55 nm (simulation 2). The lateral box dimensions showed no significant drift to new equilibrium values.

During the formation process it appears that the pore is stabilized by additional water molecules. Approximately 5–10 water molecules seem to be directly attached to the constrained (partial) pore, the major part of them at the
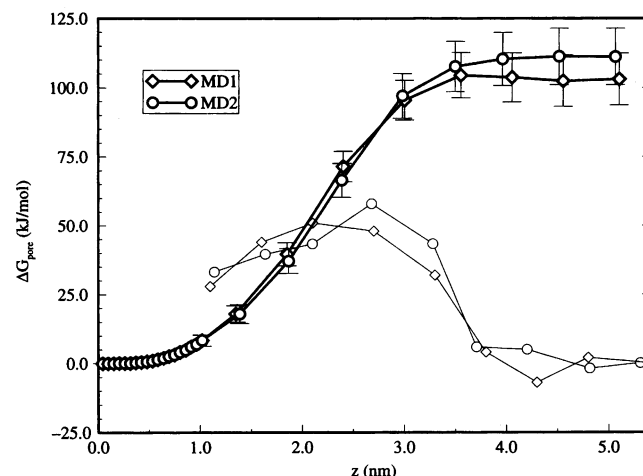

FIGURE 4 Excess free energy of the formation of a water pore in a lipid membrane. The first part of the free energy curves (high dot density) is based on the free energy of single water molecules (Marrink and Berendsen, 1994); the remaining part is computed with the coupling method. The average constraint forces at the nine stages of pore formation are also shown (thinner curves).

beginning of the pore. Apart from these directly attached water molecules, Fig. 3 shows that the pore opening is further stabilized by an increase in the number of water molecules in region 2, adjacent to the penetrating strand. The surrounding lipid headgroups at both edges of the pore seem to bend only slightly toward the pore-attached cluster of water molecules. Larger stabilizations, with water molecules attached throughout the whole pore and with lipids headgroups adjacent to the pore, are not observed.

Free energy of pore formation

The excess free energy profile of pore formation is shown in Fig. 4. The mean constrained forces from which the profile is constructed (Eq. 25) are also shown. The periods of 100-ps simulation time of the different pore stages turned out to be long enough to yield stable results. The results of the two independent simulations agree very well, within the error bars of $\sim$10 kJ/mol. The total excess free energy for the full water pore is computed to be 108($\pm$10) kJ/mol. Although the formation of the pore seems to be stabilized by reaching the other side of the membrane (look also at the constraint forces), no apparent activation barrier is observed. If the error bars are taken into account, the activation energy for pore formation equals the excess free energy.

Per pore molecule, the average free energy is 6.4 kJ/mol. This value can be compared with the average value of the

excess free energy of a single permeating water molecule in the membrane, which is $\sim$12.5 kJ/mol (Marrink and Berendsen, 1994). The free energy gain of combining water molecules into a pore conformation results obviously from the possibility for the pore molecules to make hydrogen bonds, especially in the hydrophobic part of the membrane.

Water pore conformations

The full water pore was sampled during an additional 160-ps run for both simulations. We applied the same restraints as during the formation of the pore to be able to sample tHBC conformations only. From these runs statistical data were obtained involving hydrogen-bonding characteristics and dipole orientations of the tHBC. In Fig. 5 the average number of nearest-neighbor water molecules $<n_{NEIGHB}>$, the average number of interwater hydrogen bonds $<n_{HBONDS}>$, and the average dipolar orientation $<Dip>$ of each of the individual pore molecules are plotted. The results are shown for both simulations.

From the number of nearest-neighbor water molecules of the pore molecules it appears that the middle eight waters are (almost) not stabilized by additional waters. The number of nearest neighbors remains close to two, the adjacent pore molecules. The width of this region of eight water molecules measures on average 2.5 nm and thus coincides with the hydrophobic regions 3 and 4 of the membrane as defined
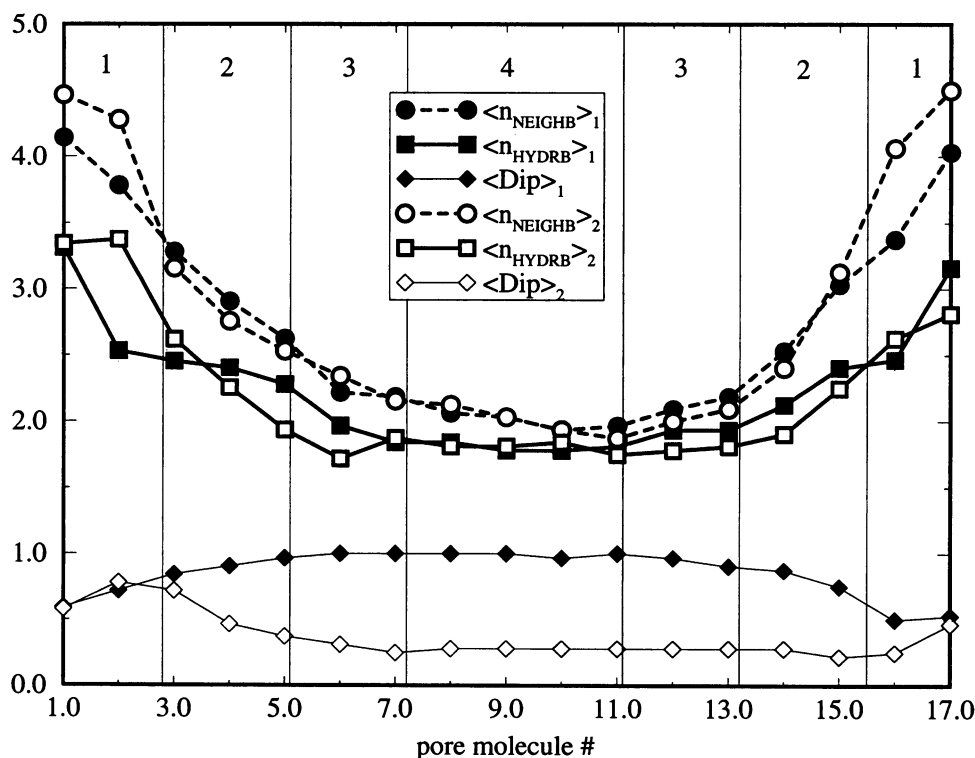

FIGURE 5　Pore conformation characteristics of both simulations. The vertical lines indicate different membrane regions. The number of nearest neighbors was computed by use of a cutoff radius of 0.36 nm, corresponding to the first minimum in the radial distribution function. For the hydrogen bonds a cutoff of 10 kJ/mol for the pair energy was used. The dipolar orientation is simply defined as being 1 for a water dipole oriented toward one side of the membrane and 0 for orientation toward the opposite side.

in the four-region model (Marrink and Berendsen, 1994; Marrink, 1994). The pore molecules that reside in region 2 are stabilized on average by at least one additional water molecule. Toward region 1 this number increases further, toward the bulk value 4.8 of SPC water. The number of hydrogen bonds per pore molecule parallels the number of nearest neighbors to a large extent. Especially in the middle of the membrane the fraction of neighboring pore molecules that are hydrogen bonded is close to 1.

The dipolar orientation of the water molecules in the pore is remarkable. In simulation 1 the water molecules remain completely oriented toward one direction during the whole simulation of 160 ps. Only the pore molecules in the more aqueous surrounding of region 1 show a more random orientation (indicated by a value of 0.5). The situation in simulation 2 is different, however. In this case most of the pore molecules have an average dipolar orientation of $\sim$0.3, which means that 70% of the time they are oriented toward one direction and 30% of the time toward the opposite direction. Whether random transitions of individual water molecules or cooperative transitions of the whole pore have taken place is not clear from these data, but below we will show that a single cooperative transition has taken place after $\sim$30% of the total simulation time.

The time evolution of the number of hydrogen bonds and of the dipolar orientation of the pore molecules gives insight into the dynamic aspects of the pore conformations. In Fig. 6 we plot the number of hydrogen bonds and the dipolar orientation averaged over the middle eight pore molecules. We selected the middle eight water molecules only, because these are the "hydrophobic" ones, which are connected only to one another. These molecules will be essential for the proton transport; i.e., they form the bottleneck.

From Fig. 6 it is clear that the essential part of the water pore remains almost fully hydrogen bonded throughout the simulation time. The average number of hydrogen bonds for the "hydrophobic" pore molecules is $\sim$1.8 in both simula-
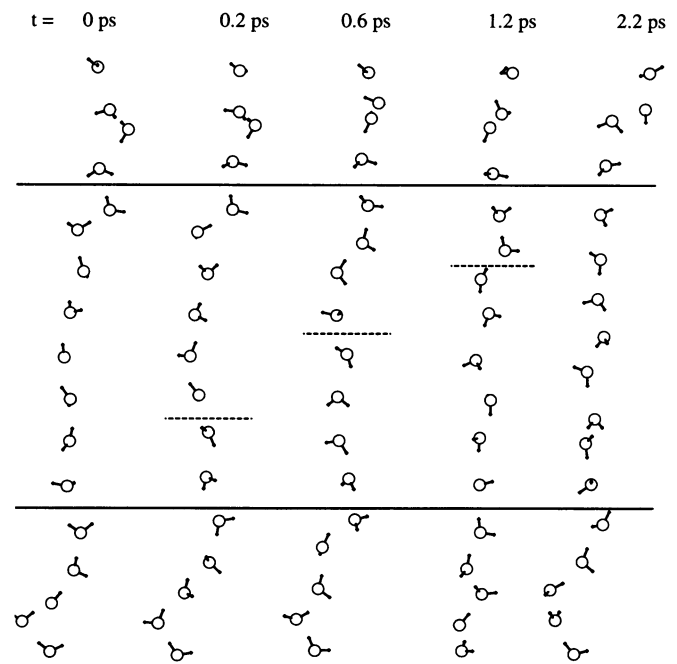
FIGURE 7   Sequence of five snapshots of the water pore during the transport of a turning defect. The location of the turning defect is marked by a dashed line. The water molecules between the two solid lines are the "hydrophobic," or essential, ones.

tions. To be able to transport a proton by means of the translocation mechanism, the pore should be hydrogen bonded throughout, implying two hydrogen bonds per molecule. This is achieved only in 35% (simulation 1) and 28% (simulation 2) of the total simulation time.

In the same figure, the time evolution of the dipolar orientation of the "hydrophobic" pore molecules very nicely shows the appearance in simulation 2 of a cooperative transition from a pore oriented toward one direction to a pore oriented toward the opposite direction. The transition itself takes place very rapidly, within 2 ps. The net effect of this process is the transport of a turning defect. To illustrate this process further, we have plotted in Fig. 7 a few pore conformations that appear during this transition (compare also Fig. 1 B).

Fig. 7 shows that the turning defect is translocated in a rather linear way. No diffusive process is observed. Apparently, once the defect is created it can move very rapidly along the hydrogen-bonded chain of water molecules. Within a period of $\sim$2 ps the essential water molecules have all changed from an orientation toward one direction (leftmost conformation) to an orientation toward the opposite direction (rightmost conformation). However, the observation of only one such a transition during 320 ps of simulation indicates that the initial formation of the turning defect is a slow process.

Water pore stability

To compute the stability of the water pore we performed some additional simulations, starting from conformations
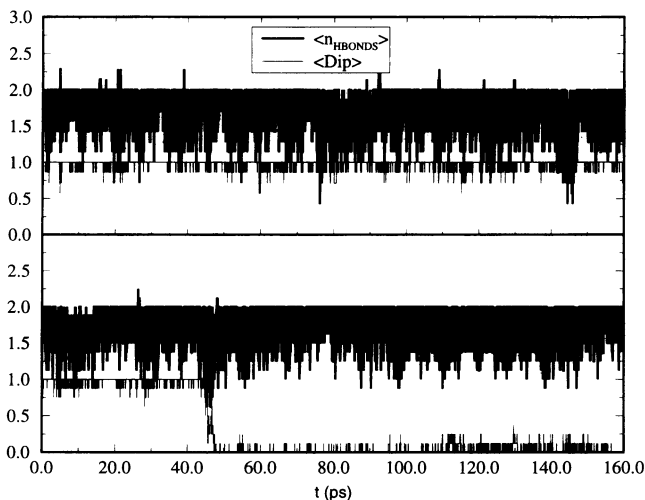

FIGURE 6   Time evolution of pore characteristics. Upper figure, simulation 1; lower figure, simulation 2. See the caption to Fig. 5 for definitions.
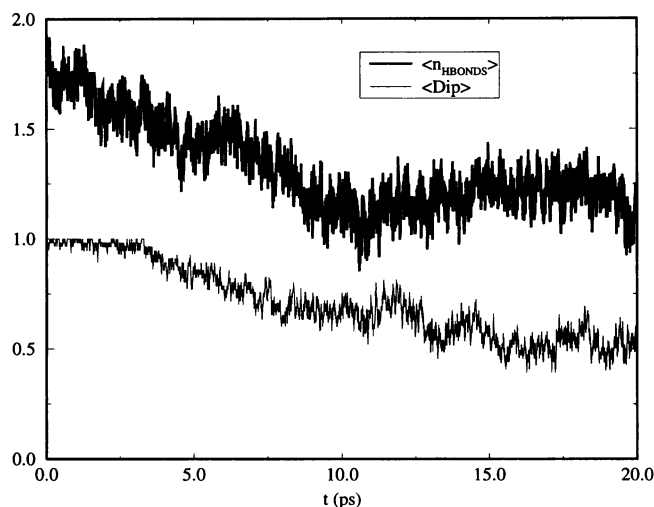
FIGURE 8   Time evolution of pore characteristics during unconstrained simulations. Data are averaged over 16 independent simulations. See the caption to Fig. 5 for definitions.

generated during the 160-ps runs of the full pore. Every 20 ps we restarted the simulations, but now with removal of all constraints that were previously applied to the pore. Assuming that the reduction of the pore is a process that is much less costly in free energy terms than its formation, we anticipated that it should be feasible within short simulations to observe the breakdown of a pore. In practice it turned out that 20-ps simulations were enough in all cases to yield pore conformations that had so many defects that proton transport would be impossible.
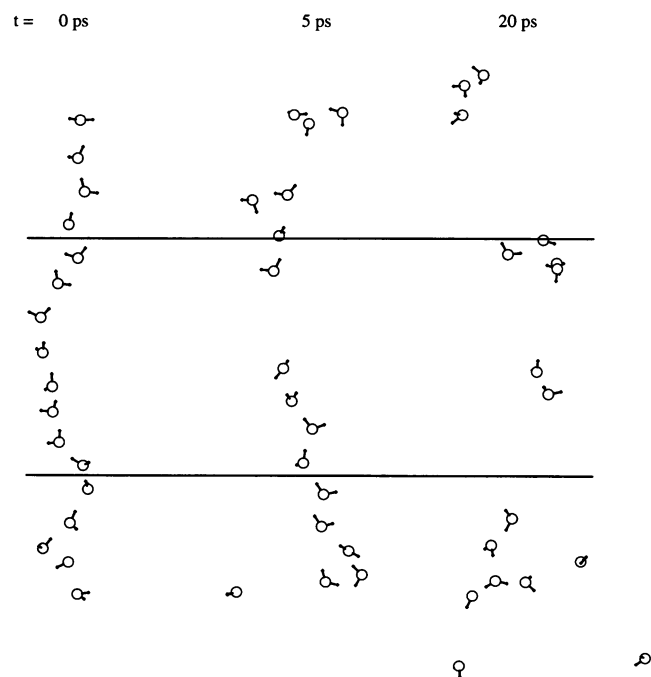

FIGURE 9   Example of a pore reduction process. The solid lines indicate the boundaries between the hydrophobic and the hydrophilic parts of the membrane.

The time evolution of hydrogen bonds and dipolar orientation of the essential (i.e., middle eight) water molecules were analyzed for all 16 unconstrained simulations. The average results are presented in Fig. 8.

The decay both of the average number of hydrogen bonds and of the average dipolar orientation is clearly observable. The number of hydrogen bonds decreases immediately, and after 3 ps a substantial number of turning defects start to appear. The longest observed time for a fully hydrogen-bonded chain to persist was 5 ps. Most pores already had ceased to exist as such after 2 ps.

A typical example of the process of pore reduction is shown graphically in Fig. 9. One sees that after 5 ps two large gaps already exist, with clearly broken hydrogen bonds. The conformation after 20 ps shows that the water pore has broken down into several small clusters. The outer two parts of the pore are immediately pulled back into the water layer. The other clusters will (probably) spend some more time in the bilayer core before dissolving into the water layer at either side.

The low stability of the pore is in agreement with the free energy calculations, which show that no substantial activation energy barrier is present between the full pore and the dissolved pore (see Fig. 4). The thermal energy of the pore molecules and the lipid surroundings is already sufficient to break down the interpore hydrogen-bonded structure.

Rate constants

Now that the complete analysis of the simulation results has been presented, we can compute the various rate constants that are important for computing the overall rate of proton transport by the pore mechanism.

The rate of ionic translocation, k_{ID}, can be calculated from Eqs. 29 and 30. The width of the water pore required for calculating the excess Born energy of the "proton" (i.e., a charge of $0.62e$) in the pore can be estimated from the average number of nearest neighbors of the pore. Only the pore width in the hydrophobic part of the membrane has to be considered; the excess Born energy in the hydrophilic parts will be negligibly small. From the data that are presented in Fig. 5 we calculated that, on average, the pore is stabilized by $0.3(\pm 0.1)$ water molecules in region 3 and by $0.1(\pm 0.1)$ water molecules in region 4. Taking the diameter of a water molecule as 0.3 nm, we can use Eq. 30 to compute the excess free energy. We find an excess free energy barrier needed for the ionic translocation step of $12(\pm 1)$ kJ/mol in region 3 and of $14(\pm 2)$ kJ/mol in region 4. The Boltzmann-weighted average over the whole membrane (including regions 1 and 2 for which we stated that $\Delta G_{prot} \approx 0$ kJ/mol) is $11(\pm 1)$ kJ/mol. The rate of the ionic translocation step now follows from Eq. 29. Using $k_{ice} = 10^{11}$ s^{-1}, we calculate that $k_{ID} = 2(\pm 1) \times 10^9$ s^{-1}. As discussed above, k_{ID} can be much faster in the case of the recombination mechanism.

The rates of proton–pore association and dissociation depend on the width of the pore opening (Eqs. 31 and 32).

From our simulation results it follows that the opening of the pore is stabilized by a number of water molecules occupying an area with a diameter of $\sim 1.0(\pm .5)$ nm (see Fig. 3). Thus it is reasonable to assume that protons reaching this region are sensitive for the ionic translocation mechanism across the pore. Substituting $d_{pore} = 1$ nm and $D_{prot} = 10^{-4}$ cm^2 s^{-1} into Eqs. 31 and 32 yields $k_a = 8(\pm 4) \times 10^{13}$ mol^{-1} cm^3 s^{-1} and $k_d = 8(\pm 6) \times 10^{10}$ s^{-1}.

The rate of the turning defect translocation, k_{TD}, can be estimated from the number of times that the transition between the two possible pore orientations occurred spontaneously during the full pore simulations. This has happened exactly one time, in a period of 320 ps, implying that $k_{TD} \approx 3 \times 10^9$ s^{-1}. Because only one such an event has been observed, the statistical information is of course very poor. Nevertheless, it provides us with a rough estimate of the order of magnitude of the turning defect translocation rate. It can be compared with the result obtained by Pomès and Roux (1996b) in their simulation of a water wire inside the gramicidin channel. They observed the occurence of turning defect translocations also, on a time scale of several hundred picoseconds. They concluded that the local interaction of especially the outermost water molecules with the channel atoms slowed down the translocation of the turning defect. In accordance with this observation we have seen that, once one of the outermost water molecules changed its polarization, the other ones followed very quickly (Fig. 7).

The reduction rate constant of the water pore, k_R, can be directly obtained from the average lifetime of the unconstrained pore, which we estimated as $3(\pm 1)$ ps (see the discussion of Fig. 8). Expressed as a rate, it is thus $k_R = 3(\pm 1) \times 10^{11}$ s^{-1}.

From the excess free energy of pore formation and the rate of pore reduction it is now possible to compute the rate of pore formation k_F by use of Eq. 21. Using the calculated excess free energy of $108(\pm 10)$ kJ/mol, the simulation temperature of 350 K, and a water surface density of 17×10^{-10} mol cm^{-2}, we find that the probability p_{pore} of a water pore to exist in the membrane is between 3×10^{-27} and 3×10^{-24} mol cm^{-2} membrane surface. Note, however, that this probability concerns all possible pore conformations, including those that are not completely hydrogen bonded. We have shown that on average approximately one third of the sampled pore conformations are completely hydrogen bonded, i.e., appear as tH-BCs. Assuming that only the tHBCs are able to conduct protons, the required probability of pores drops to a value between 1×10^{-27} and 1×10^{-24} mol cm^{-2} membrane surface. With the estimated reduction rate constant k_R given above, the rate of pore formation becomes $3 \times 10^{-16} < k_F < 3 \times 10^{-13}$ mol cm^{-2} s^{-1}.

DISCUSSION

Proton transport

Thus far, we have shown that it is possible to simulate a slow process, the formation of a water pore in a lipid

membrane, successfully with the MD method. We have been able to extract various rate constants that are important in the process of the (hypothetical) proton transport across such a pore. Although some additional assumptions have been made, the predicted rate constants are expected to indicate the correct order of magnitudes of the various steps. Before turning toward the implication of the results for the actual proton transport rate, we will first discuss the nature of the pore itself.

The height of the free energy barrier of pore formation, more than 100 kJ/mol, indicates that such a complete water pore spanning the membrane is a rare phenomenon. Direct detection of such pores with experimental techniques seems therefore impossible. In a lipid vesicle with a diameter of 0.2 μm, only 100 pores suitable for transporting protons would be formed per second. Comparing the various rate constants makes clear that once a pore has been formed it is only very short lived, with an average lifetime of less than 5 ps. This time is much shorter than the time required for a turning defect to occur. In practice this means that a water pore can transport only one proton, after which it will almost certainly be reduced. The nature of the pore is thus very transient.

Comparing k_{ID} with k_D shows that the ionic translocation step is relatively slow, and the transport of the proton across the pore becomes activation controlled, with overall rate constant $k_2 = k_{ID}k_a/k_d$ of the order of 10^{12} mol^{-1} cm^3 s^{-1}. If we assume that in the case of the recombination mechanism k_{ID} is much faster, than the rate becomes diffusion controlled, implying that $k_3 = k_a = 8(\pm 4) \times 10^{13}$ mol^{-1} cm^3 s^{-1}. Comparison of k_3 with k_2 shows that the necessary condition for the recombination mechanism $k_3 K_w \gg k_2[H^+]$ can never be obtained at normal pH values. Therefore our simulations predict that the recombination mechanism will always be dominated by the uncoupled mechanism.

We will now turn to the main question: Is the occasional presence of very transient water pores in the membrane able to account for the large proton transport rate? Substituting the rate constants that we have calculated straightforwardly into Eqs. 11 and 17 yields clearly negative answers. Considering a concentration difference of 0.1 μM and an ambient pH of 7, the application of Eq. 11 results in a proton flux of only $J_{prot} \sim 10^{-23}$ mol s^{-1} cm^{-2} membrane surface. The experimentally predicted value for the same driving concentration difference is of the order of 10^{-15} mol s^{-1} cm^{-2}. This is ~ 8 orders of magnitude faster. Moreover, the permeability coefficient is predicted to be independent of the ambient pH, as in normal types of permeation processes. The recombination mechanism, Eq. 17, gives, as anticipated, even a much lower proton flux: $J_{prot} \sim 10^{-31}$ mol s^{-1} cm^{-2}. In this case, however, the pH dependence is in agreement with the experimental observation.

The failure of the pore mechanism to account for the fast proton transport rates lies in the transport rate of the proton across the pore, k_2. This step requires that a proton enter the pore and subsequently be translocated to the other side. This is

a second-order process, implying that the total rate constant is determined by the product $k_2[H^+]$ (or $k_3 K_w$ in the case of the recombination mechanism). At relevant pH values the concentration of protons is very low, and the product becomes orders of magnitude too small. Possibly, the rate of transport of the ionic defect k_{ID} is much faster than computed. Equation 29 is based on a diffusive kind of motion across a free energy barrier. As we have seen with the observed translocation of the turning defect, the water molecules in the pore are able to reorient in a highly cooperative way. Also, the computer simulations of Pomès and Roux (1996a,b), which use a much more sophisticated model, show that cooperative effects result in a very fast translocation rate. The quantitative predictions from Eq. 29 should therefore not be considered too strictly. In the case of the recombination of a proton–hydroxide pair the speed of proton translocation can even be further increased. However, even if the translocation step itself were infinitely fast, the entering of the proton at the pore itself would become rate limiting, because this is still a diffusion-controlled process.

The only possible way in which this single-file pore mechanism can work is that somehow the process of protons entering the pore is much faster. If k_a is at least 8 orders of magnitude faster (and also k_{ID}; otherwise the process again becomes activation controlled), then Eq. 11 reduces to Eq. 12, i.e., tHBC model II, which has the correct pH dependence and which predicts a proton transport flux of $J_{prot} \sim 10^{-14}$ mol s^{-1} cm^{-2}, in close agreement with the experimental results. The rate-limiting step is now the formation of the pore. Once the pore has been formed it is able to transport a single proton, whereafter it breaks down. For model IIa, for which Eq. 17 also reduces to Eq. 12, almost relativistic rates of proton delivery are required. But, even then, the recombination mechanism will turn out to be slower than the uncoupled mechanism.

How can protons or hydroxide ions be so effectively delivered that every time a pore forms a proton is indeed being translocated? A possible explanation is that the effective concentration of protons close to the pore is much larger than the ambient pH. This could be the case if the pore is most likely to form at a place where protons or hydroxide ions are present. Such a preference could result from the spatial fluctuations of the electric field related to the ionic distribution. The observed dipole alignment in the water pore underlines the importance of electrostatic interactions within the membrane. Another possibility would be that the pore opening is much larger or is extending into the solvent via hydrogen-bonded pathways. Also, the existence of nondiffusive pathways for protons to enter the pore has been proposed by Deamer and Nichols (1989). Special conductance pathways along lipid headgroups or generation of proton–hydroxide pairs by means of the water equilibrium are mentioned. The most promising assumption, however, is that the effective concentration of protons is much higher because of the presence of buffers. Suitable lipid headgroups can themselves act as buffers, and most experimental measurements of proton flux have mobile buffers present, typically in the range of 10–100 mM, which is 5–6

orders of magnitude higher than the proton concentration at pH 7. The presence of concentrated buffers was also used by Benz and Mclaughlin (1983) to account for the proton conduction by the protonophore FCCP, in which case protons were also delivered at a rate much faster than expected by simple diffusion. If buffers are indeed present in such high concentrations near the membrane, than the proton delivery problem is (almost) solved, as protons can easily be donated to the pore by these buffers. If the assumptions are correct, a combination of these explanations is certainly sufficient to make the pore mechanism realistic.

Error discussion

The computation of the various rate constants is of course subject to several sources of error that are due partly to the assumptions that have been made and partly to the limitations of the computational procedures. We will now briefly discuss the possible effects of these errors on the conclusions that have been drawn in the previous section.

The two independent simulations of water pores that we conducted offer a strong test for the reliability of the results. The reported error bars in the calculations are based on the differences between the two simulations. For some properties (such as stabilization of the pore by adjacent water molecules) the quality of the information could be further enhanced by comparison of the two halves of the bilayer. For most rate constants the resulting statistical errors confine an order of magnitude, which is accurate enough considering on one hand the crude underlying theoretical models and on the other hand the kinds of conclusions that we would like to draw.

The reported error in the computation of the free energy of pore formation of 10 kJ/mol is based on the integrated error of the average constrained forces. The difference between the two simulations remains within this error. However, we have to keep in mind that we have simulated a mesoscale process, the formation of a water pore in the membrane, for a microscale time, and systematic errors could emerge. The long simulation period (1080 ps to create the pore) is in principle long enough to allow for larger deformations of the membrane components, such as large thinning defects. The absence of larger stabilizations indicates that deformations of the lipid membrane structure are too costly in terms of free energy. Also, in the subsequent 160-ps simulation of the full pore the degree of stabilization did not change, nor did the box dimensions. Nevertheless, fluctuations in the membrane that occur on the microsecond time scale are inaccessible. Such rare fluctuations could be important for the free energy profile, and one can therefore not exclude that the actual formation of a water pore in a real membrane is less costly in terms of free energy.

Another factor that might influence the height of the free energy barrier is the temperature. Our simulation temperature is 350 K, which is well above the main phase transition temperature of 315 K. One could argue that at lower tem-

peratures the formation of a water pore becomes more likely, because the entropy of pore formation will certainly be negative. At even lower temperatures, below the main phase transition, the enthalpy barrier becomes much larger, and the formation of a water pore becomes less likely. Also, at lower temperature the rate of pore reduction will be slower. The nature of the pore will remain very transient, though. The precise value of the lifetime is hard to define but is not important as long as it is much smaller than the translocation time for the hopping defect. As an upper limit we can assume 10 ps. This still requires an anomalous diffusion mechanism of protons to the pore.

A different factor with important kinetic consequences would be the presence of multifile water pores. A multifile water pore could perhaps be formed without too much additional free energy. Although a multifile water pore did not form spontaneously in our simulations, we cannot rule out that it can occur on larger time scales. For a multifile water pore the rate of reduction will become much smaller. The translocation rate of the turning defect will drop out of the kinetic equations, as there will always be a suitably oriented hydrogen-bonded chain in such a multifile pore. Will such a pore be able to account for the observed proton transport rates? For the correct pH dependency to be obtained, its stability should be of the order milliseconds (i.e., $k_R \approx 10^3 \text{ s}^{-1}$), and Eq. 12 can be applied. However, with such a slow reduction rate the pore formation rate will also drop considerably. Therefore the predicted proton transport rate, $J = 10^{-21} \text{ mol cm}^{-2} \text{ s}^{-1}$, is still ~6 orders of magnitude too slow. Bringing the experimental and theoretical values together would require an additional stabilization of ~35 kJ/mol of the free energy of pore formation. Dissolving at least 50 water molecules (needed to construct a multifile water pore) in the membrane at the cost of only slightly more than 70 kJ/mol does not seem realistic, however. Besides, other ions would also benefit from such a pore, and the large difference between ion and proton permeation rates remains unexplained.

CONCLUSION

We have presented the results of two independent MD simulations of a phospholipid membrane in which a single-file water pore was slowly formed. The water molecules within the pore act in a very cooperative way, with all dipoles aligned in the same direction. Both pore ends are stabilized by an additional number of water molecules, leaving approximately eight pore molecules in the hydrophobic part of the membrane that are hydrogen bonded only to one another. These water molecules are the essential ones for the proton transport process. From the excess free energy of water pore formation we conclude that the equilibrium density of a water pore in a membrane is very small. Moreover, if such a pore is formed, its lifetime will only be a few picoseconds. Whether the presence of these occasional, very transient pores can still account for the high

proton fluxes that are experimentally observed depends on the rate at which protons can be donated at the pore. Only when every time that a pore is formed a proton indeed is translocated is the predicted proton flux and concentration dependence in agreement with the experimental data. Because the proton concentration near pH 7 itself is too low for the protons to be delivered at the required rate, the presence of concentrated buffers near the membrane has to be assumed to make the pore mechanism realistic.

REFERENCES

Benz, R., and S. McLaughlin. 1983. The molecular mechanism of action of the proton ionophore FCCP. Biophys. J. 41:381–398.

Cafiso, D., and W. Hubell. 1983. Electrogenic proton/hydroxide movement across phospholipid vesicles measured by spin-labeled hydrophobic ions. Biophys. J. 44:49–57.

Deamer, D. W. 1987. Proton permeation of lipid bilayers. J. Bioeng. Biomembr. 19:457–478.

Deamer, D. W., and J. Bramhall. 1986. Permeability of lipid bilayers to water and ionic solutes. Chem. Phys. Lip. 40:167–188.

Deamer, D. W., and J. W. Nichols. 1983. Proton-hydroxide permeability of liposomes. Proc. Natl. Acad. Sci. USA. 80:165–168.

Deamer, D. W., and J. W. Nichols. 1989. Proton flux mechanisms in model and biological membranes. J. Membr. Biol. 107:91–103.

Deamer, D. W., and A. G. Volkov. 1995. Proton permeation of lipid bilayers. In Permeability and Stability of Lipid Bilayers, E. A. Disalvo and S. A. Simon, editors. CRC Press, Boca Raton, FL. 161–178.

Egberts, E., S. J. Marrink, and H. J. C. Berendsen. 1994. Molecular dynamics simulation of a phospholipid bilayer. Eur. Biophys. J. 22:423–436.

Elamrani, K., and A. Blume. 1983. Effect of lipid phase transition on the kinetics of H^+/OH^- diffusion across phosphatidic acid bilayers. Biochim. Biophys. Acta. 727:22–30.

Flewelling, R. F., and W. L. Hubbell. 1986. The membrane dipole potential in a total membrane potential model. Applications to hydrophobic ion interaction with membranes. Biophys. J. 49:541–552.

Georgallas, A., J. D. MacArthur, X. P. Ma, C. V. Nguyen, G. R. Palmer, M. A. Singer, and M. Y. Tse. 1987. The diffusion of small ions through phospholipid bilayers. J. Chem. Phys. 86:7218–7221.

Gutknecht, J. 1984. Proton/hydroxide conductance through lipid membranes. J. Membr. Biol. 82:105–112.

Gutknecht, J. 1987a. Proton conductance through phospholipid bilayers: water wires or weak acids? J. Bioeng. Biomembr. 19:427–442.

Gutknecht, J. 1987b. Proton/hydroxide conductance and permeability through phospholipid bilayer membranes. Proc. Natl. Acad. Sci. USA. 84:6443–6446.

Gutknecht, J., and A. Walter. 1981. Transport of protons and hydrochloric acid through lipid bilayer membranes. Biochim. Biophys. Acta. 641:183–188.

Hamilton, R. T., and E. W. Kaler. 1990. Alkali metal ion transport through thin bilayers. J. Phys. Chem. 94:2560–2566.

Hauser, H., D. Oldani, and M. C. Phillips. 1973. Mechanism of ion escape from phosphatidylcholine and phosphatidylserine single bilayer vesicles. Biochemistry. 12:4507–4517.

Marrink, S. J. 1994. Permeation of small molecules across lipid membranes. Ph.D. Thesis. University of Groningen. 167 pp.

Marrink, S. J., and H. J. C. Berendsen. 1994. Simulation of water transport through a lipid membrane. J. Phys. Chem. 98:4155–4168.

Marrink, S. J., and H. J. C. Berendsen. 1996. Permeation process of small molecules across lipid membranes studied by molecular dynamics simulations. *J. Phys. Chem.* (submitted).

Marrink, S. J., M. Berkowitz, and H. J. C. Berendsen. 1993. Molecular dynamics simulation of a membrane/water interface: the ordering of water and its relation to the hydration force. *Langmuir.* 9:3122–3131.

Mueller, P., D. O. Rudin. 1967. Action potential phenomena in experimental bimolecular lipid membranes. *Nature.* 213:603–604.

Nagle, J. F. 1987. Theory of passive proton conductance in lipid bilayers. *J. Bioeng. Biomembr.* 19:413–426.

Nagle, J. F., M. Mille, and H. J. Morowitz. 1980. Theory of hydrogen bonded chains in bioenergetics. *J. Chem. Phys.* 72:3959–3971.

Nagle, J. F., and H. J. Morowitz. 1978. Molecular mechanisms for proton transport in membranes. *Proc. Natl. Acad. Sci. USA.* 75:298–302.

Nagle, J. F., and Tristam-Nagle, S. 1983. Hydrogen bonded chain mechanism for proton conduction and proton pumping. *J. Membr. Biol.* 74:1–14.

Nichols, J. W., and D. W. Deamer. 1980. Net proton-hydroxyl permeability of large unilamellar liposomes measured by an acid-base titration technique. *Proc. Natl. Acad. Sci. USA.* 77:2038–2042.

Nichols, J. W., M. W. Hill, A. D. Bangham, and D. W. Deamer. 1980. Measurement of net proton-hydroxyl permeation of large unilamellar liposomes with the fluorescent pH probe 9-aminoacridine. *Biochim. Biophys. Acta.* 596:393–403.

Nozaki, Y., and C. Tanford. 1981. Proton and hydroxide ion permeability of phospholipid vesicles. *Proc. Natl. Acad. Sci. USA.* 78:4324–4328.

Parsegian, A. 1969. Energy of an ion crossing a low dielectric membrane: solutions to four relevant electrostatic problems. *Nature.* 221:844–846.

Paula, S., G. Volkov, N. van Hoek, T. H. Haines, and D. W. Deamer. 1996. Permeation of protons, potassium ions, and small polar molecules through phospholipid bilayers as a function of membrane thickness. *Biophys. J.* 70:339–348.

Perkins, W. R., and D. S. Cafiso. 1986. An electrical and structural characterization of H^+/OH^- currents in phospholipid vesicles. *Biochemistry.* 25:2270–2276.

Pines, E., and D. Huppert. 1985. Kinetics of proton transfer in ice via the pH-jump method: evaluation of the proton diffusion rate in polycrystalline doped ice. *Chem. Phys. Lett.* 116:295–301.

Pomès, R., and B. Roux. 1996a. Theoretical study of H^+ translocation along a model proton wire. *J. Phys. Chem.* 100:2519–2527.

Pomès, R., and B. Roux. 1996b. Structure and dynamics of a proton wire: a theoretical study of H^+ translocation along a single file water chain in the gramicidin channel. *Biophys. J.* In press.

Scheiner, S., and J. F. Nagle. 1983. Ab initio molecular orbital estimation of charge partitioning between Bjerrum and ionic defects in ice. *J. Phys. Chem.* 87:4267–4272.